Valence-band mixing in neutral, charged, and Mn-doped self-assembled quantum dots

Y. Léger, L. Besombes, L. Maingault, and H. Mariette
Institut Néel, CNRS and Université Joseph Fourier, 25 avenue des Martyrs, BP 166, 38042, Grenoble cedex 9, France
(Received 12 February 2007; revised manuscript received 25 April 2007; published 24 July 2007)

We analyze the optical emission of single II-VI quantum dots containing 0 or 1 magnetic atom (manganese) and a controlled number of carriers (0, ±1 electron). The emission of these quantum dots presents a large degree of linear polarization. This linear polarization is attributed to a valence-band mixing and we show that in nonmagnetic quantum dots combining both a shape anisotropy and an anisotropic in-plane strain distribution, the linear polarization direction of the exciton are controlled by an interplay between valence-band mixing and electron-hole (e-h) exchange interaction. Similarly, under strong transverse magnetic field, the direction of the linearly polarized emission of the charged excitons is simultaneously controlled by the valence-band mixing and the direction of the magnetic field. In quantum dots containing a Mn atom, the valence-band mixing allows simultaneous hole-Mn spin flips coupling bright and dark excitons. These spin flips are responsible for linearly polarized transitions in the emission of the charged excitons at zero magnetic field.

DOI: 10.1103/PhysRevB.76.045331 PACS number(s): 78.67.Hc, 78.55.Et, 75.75.+a

I. INTRODUCTION

The control of an individual spin in a solid state environment has attracted a lot of interest in the recent years. An individual spin in a solid is a potential candidate for the realization of quantum information processing devices. In this context, the spins of electronically charged quantum dots (QDs) are especially exciting because of their long coherence time. The incorporation of magnetic impurities in the QDs adds an additional degree of freedom for the spin manipulation[1] and could be a way to increase the spin relaxation time of the confined carriers at zero external magnetic field. However, in real self-assembled QDs, the ground eigenstates are not usually pure spin eigenstates. A detailed knowledge of the spin structure of charged QDs and the ability to control the individual spin state of the dots are essential for the development of these spin based devices.

In this work, using the optical emission of neutral and charged excitons as a probe, we examine the influence of the QD symmetries on the carrier eigenstates and on their exchange coupling with the spin of a Mn atom. In self-assembled QDs grown on [001] axis, the growth direction (z) defines a quantization axis for the holes and the symmetry of the bulk semiconductor implies that the x and y directions are equivalent. This equivalence is usually lifted by the reduced symmetry of actual QDs. The in-plane anisotropy of the confinement potential combined with the electron-hole (e-h) exchange interaction splits the bright excitons into a linearly polarized doublet. The linear polarization directions are defined by the principal axes of the confinement potential.[2] On the other hand, an anisotropic strain distribution in the QD plane produces, through the Bir-Pikus Hamiltonian, a mixing of light-hole (lh) and heavy-hole (hh) subbands. This valence-band mixing (VBM) is responsible for a linear polarization degree of the QD emission[3] with a linear polarization direction imposed by the strain distribution.

Here, the emission of neutral exciton X, negatively charged excitons X^-, and positively charged exciton X^+ coupled or not with a single magnetic atom is observed in individual QDs. We show that in II-VI QDs combining both a shape anisotropy and an anisotropic in-plane strain distribution, the linear polarization directions of the neutral exciton are controlled by an interplay between VBM and e-h exchange interaction. Similarly, under strong transverse magnetic field, the linearly polarized emission of the charged excitons is simultaneously controlled by the VBM and the magnetic coupling of the holes. In QDs containing a magnetic atom, the VBM significantly affects the coupling between the confined hole and the localized magnetic moments. It allows simultaneous hole-Mn spin flips responsible for a coupling between the dark and bright exciton states at zero magnetic field and the appearance of linearly polarized transitions in the charged exciton emission.

In this article, we first present the studied QD samples and the method used to tune the dominant charge state of the dots (Sec. II). Then we present a description of the main parameters influencing the lh-hh mixing in self-assembled QDs (Sec. III). In Sec. IV, we analyze the effect of the interplay between the strained-induced valence-band mixing and the e-h exchange interaction. The next section (Sec. V) deals with the interplay between the in-plane anisotropy induced by the VBM and the controlled anisotropy introduced by a transverse magnetic field. Finally, we discuss the influence of the VBM on the exchange coupling between a localized Mn spin and the spin of confined carriers (Sec. VI). All the experimental results are analyzed in the framework of an effective spin Hamiltonian including the exchange interactions, the magnetic field, and the VBM induced by the local strain distribution.

II. CHARGE TUNABLE CdTe/ZnTe QUANTUM DOTS

The CdTe/ZnTe QDs samples used in this study are grown by atomic layer epitaxy by deposition of six monolayers of CdTe on a ZnTe barrier. QD formation is then induced with deposition and/or desorption of amorphous Te.[4] The height and diameter of the QDs' core are about 3 and 15 nm, respectively, as revealed by transmission electron microscopy.[5] A low density of Mn atoms can be introduced

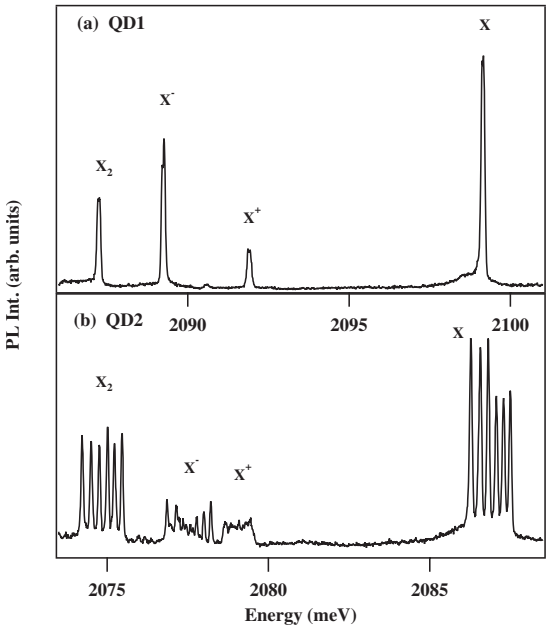

FIG. 1. (a) 5 K emission spectrum of a single CdTe/ZnTe QD (QD1). (b) 5 K emission spectrum of a single CdTe/ZnTe QD doped with a single Mn atom (QD2).

in the QDs exploiting the Mn diffusion through a ZnTe spacer layer grown on a ZnMnTe barrier.[6]

Microspectroscopy was used to study the magneto-optical properties of individual CdTe/ZnTe QDs. The low temperature (5 K) photoluminescence (PL) of single QDs is excited with the 514.5 nm line of an argon laser or a tunable dye laser and collected through a large numerical-aperture objective and aluminum shadow masks with 0.5–1.0 μm apertures. The experiments are carried out in the backward geometry with the propagation direction of the incident and emitted light parallel to the [001] growth axis. Superconductive coils are used to apply a magnetic field up to 11 T in Voigt or Faraday configuration. The PL is then dispersed by a 2 m double monochromator and detected by a nitrogen-cooled Si charged-coupled device camera or a Si avalanche photodiode.

CdTe/ZnTe QDs are *p*-type modulation doped by the transfer of holes from surface states that act as acceptors.[7,8] As illustrated in Fig. 1, depending on an applied bias voltage or on the excitation wavelength, the different charge states of the same QD can be observed. Exciton, biexciton, and positively and negatively charged excitons are observed in both magnetic and nonmagnetic individual QDs. The charged states X^+ and X^- have been identified in previous works.[28] The bounding energies of the charged species are quite similar from dot to dot allowing a reliable identification of the observed emission lines.

The occupation of the QDs can be controlled by an external bias voltage V_B on an aluminum Schottky gate with respect to a back contact on the *p*-type layer.[9] The bias dependent emission of a single QD is presented in Fig. 2(a). For increasing V_B, the surface level states, and then the Fermi level, are shifted below the ground hole level in the QDs which results in the single hole charging of the dots. The optically generated excitons then form charged excitons with the bias-induced extra hole in the QD. At zero bias or negative bias, the Fermi level is above the ground state and the QDs are likely to be neutral. However, the separate capture of photocreated electron or holes can sometimes charge the dots so that weak contributions of X^+ or X^- are often observed in the zero bias spectra. At zero bias or negative bias, the preferential injection of electrons inside the dots due to the band offset roughly balances the *p*-type doping.

At zero bias, excess electrons can also be injected in the QD using resonant optical excitation into the QD levels. Under resonant excitation (energy below the band gap of the barriers), optical transitions from delocalized valence-band states to the confined electron levels will preferentially create electrons in the QD (Ref. 10): the probability to find an excess electron in the QD is increased. As presented in Fig. 2(b), the negatively charged exciton emission is then seen for some discrete excitation energies. After the recombination of X^-, a single hole is likely to be captured to neutralize the QD and creates a neutral exciton. This neutralization process is responsible for the simultaneous observation of the neutral and charged species in the resonant spectra.

When carriers are simultaneously created in the ZnTe barrier by a weak nonresonant excitation [lower PL spectra in Fig. 2(b)], X^- progressively disappears and the contributions of X and X^+ increase. This evolution is characteristic of a photodepletion mechanism in modulation doped QDs.[11] High energy photoexcited e-h pairs are dissociated in the space charge region surrounding the negatively charged QDs. A carrier attracted into the charged QD then recombines with the carrier present in the QD. Thus photodepletion removes the charge from the QD at a rate proportional to the absorbed nonresonant excitation, leading to an increase of the PL of the neutral species. A contribution of X^+ is also observed as for pure nonresonant excitation. These two charge control mechanisms (bias voltage and resonant excitation combined with photodepletion) allow us to control the generation of neutral, negatively charged, and positively charged excitons in the same QD. A similar control can be obtained in Mn-doped QDs.[28]

III. VALENCE-BAND MIXING IN STRAINED INDUCED QUANTUM DOTS

Several phenomena can lead to the mixing between the light and heavy holes in QDs. First, the symmetry reduction due to the confinement geometry of the dot has to be considered. In this case, a hole band mixing appears through the nondiagonal terms of the Luttinger-Kohn Hamiltonian. This mixing is responsible for the linear polarization rate observed in strongly confined quantum wires.[12] A large wave function anisotropy is needed to reproduce the observed linear polarization.[13] Such anisotropy can only be obtained in a very elongated confining potential for the holes with large barriers. This is inconsistent with the observation of huge linear polarization rates in shallow CdTe/ZnTe QDs presenting a quite weak in-plane asymmetry as revealed by atomic force microscopy measurements.[6] Another origin of hh-lh mixing is the coupling of the X and Y valence-band states

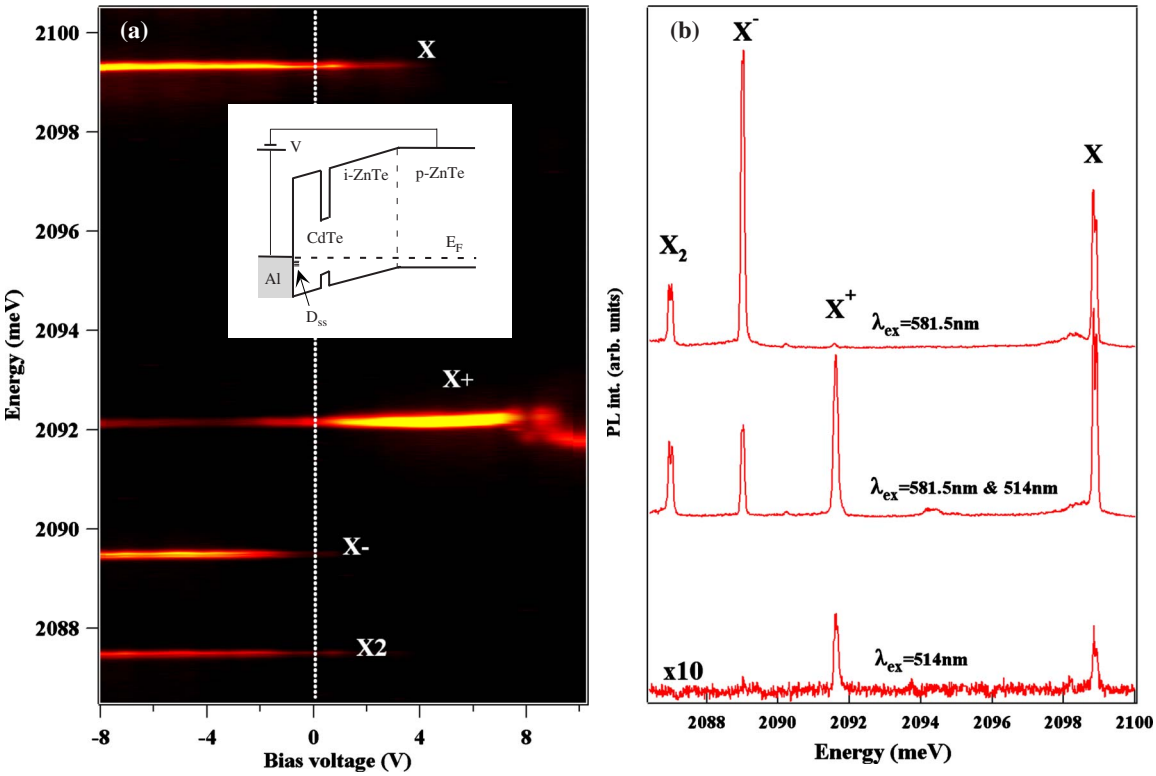

FIG. 2. (Color online) (a) Color-scale plot of the PL intensity of QD1 in a Schottky structure as a function of emission energy and bias voltage. The emission lines can be assigned to the recombination of the neutral exciton (X), biexciton (X_2), positively charged exciton (X^+), and negatively charged exciton (X^-). (b) Detail of the PL of a single QD under resonant excitation (λ_{ex}=581.5 nm), nonresonant excitation (λ_{ex}=514.5 nm) and both resonant and nonresonant excitations.

produced by the microscopic arrangement of chemical bonds at heterointerfaces.[14] This contribution is expected to be weak in flat self-assembled QDs with almost symmetric interfaces.

As we will see in the following, an efficient mixing can arise from the anisotropic relaxation of strains in the QD plane. Influence of strains on hole states has been intensively studied in quantum wells. Two main effects have been demonstrated, namely, the variation of the gap due to hydrostatic strains and the hh-lh degeneracy lift due to biaxial strains. We will show that in QDs, the strain distribution can also be responsible for a strong lh-hh mixing. This mixing has striking effects on the hole spin anisotropy.

In bulk semiconductor, the spin orbit interaction is responsible for a splitting of the hole states. We only consider here the lowest energy holes with angular momentum $j=3/2$. These $|j,j_z\rangle$ states can be simply defined using orbital (X,Y,Z) and spin $(\uparrow,\downarrow)$ eigenvectors:

$$|3/2,+3/2\rangle = -\uparrow\frac{X+iY}{\sqrt{2}},$$

$$|3/2,+1/2\rangle = \sqrt{\frac{2}{3}}\uparrow Z - \downarrow\frac{X+iY}{\sqrt{6}},$$

$$|3/2,-1/2\rangle = \sqrt{\frac{2}{3}}\downarrow Z + \uparrow\frac{X-iY}{\sqrt{6}},$$

$$|3/2,-3/2\rangle = \downarrow\frac{X-iY}{\sqrt{2}}. \quad (1)$$

Using these notations, the Bir-Pikus Hamiltonian describing the influence of the strain on the valence-band structure is written:

$$H_{BP} = -a_v\sum_i \varepsilon_{ii} - b\sum_i \varepsilon_{ii}(j_i^2 - 1/3j^2) - \frac{2d}{\sqrt{3}}\left(\varepsilon_{xy}\frac{j_x j_y + j_y j_x}{2} + \text{c.p.}\right), \quad (2)$$

where the abbreviation c.p. is used for circular permutation over x, y, and z corresponding to the crystal axes. The matrices of the angular momentum operator $\vec{j}$ can be found in Appendix A. ε_{ij} denotes the ij component of the strain tensor and a_v, b, and d are the deformation potentials for the valence-band. Using the hole formalism, Allègre *et al.* found a_v=0.91 eV, b=0.99 eV, and d=2.76 eV for CdTe.[15]

While growing CdTe on ZnTe, CdTe is compressed in the growth plane and distended in the growth direction. CdTe QDs form by deformation of a two dimensional layer induced by strain relaxation.[4] In this formation mechanism, both elastic and inelastic strain relaxations are involved and one expects each QD to probe a different local in-plane strain distribution. When studying a particular QD, one has to consider a particular set of values for ε_{ij}. In the following, we

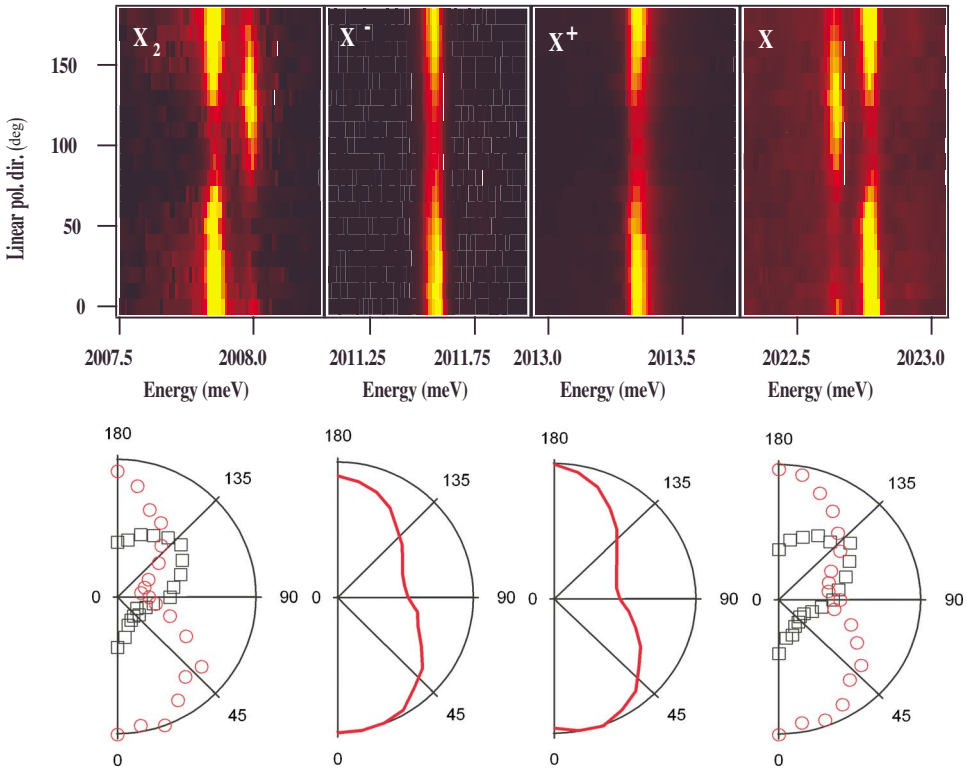

FIG. 3. (Color online) Linear polarization dependence of the PL intensity of X, X_2, X^-, and X^+ in the same QD (QD3). The polar plots depict the emission intensity for different positions of the polarization analyzer relative to [110] direction. For the exciton (biexciton), the high (low) energy line intensity is plotted with open circles and the low (high) energy line intensity is plotted with open squares.

will mainly consider the effects of strain anisotropy in the growth plane and describe the strain on each QD by average values of ε_{xy} and $\varepsilon_{xx}-\varepsilon_{yy}$. A nonzero value of the volume average ε_{ij} can result from a local deformation of the lattice induced by neighboring QDs or dislocations. In this approximation, the Bir and Pikus Himiltonian is reduced to a block-diagonal matrix in the $(+3/2, -1/2, +1/2, -3/2)$ basis:

$$H_{BP}=\begin{pmatrix} P+Q & R & & \\ R^{\dagger} & P-Q & & \\ & & P-Q & R \\ & & R^{\dagger} & P+Q \end{pmatrix}, \tag{3}$$

with

$$P=a_v\sum_i \varepsilon_{ii},$$

$$Q=b\left(\frac{\varepsilon_{xx}+\varepsilon_{yy}}{2}-\varepsilon_{zz}\right),$$

$$R=id\varepsilon_{xy}-b\frac{\sqrt{3}}{2}(\varepsilon_{xx}-\varepsilon_{yy}). \tag{4}$$

Using the hh band as the origin of the energies in the valence-band, the strain Hamiltonian can be rewritten as

$$H_{BP}=\begin{pmatrix} 0 & \rho_s e^{-2i\theta_s'} & & \\ \rho_s e^{2i\theta_s'} & \Delta_{lh} & & \\ & & \Delta_{lh} & \rho_s e^{-2i\theta_s'} \\ & & \rho_s e^{2i\theta_s'} & 0 \end{pmatrix}. \tag{5}$$

This notation allows us to introduce useful parameters to describe the strain effects, namely, the light-heavy hole splitting Δ_{lh}, the strain coupling amplitude ρ_s, and the strain-induced anisotropy axis in the QD plane defined by the angle θ_s' with respect to the x (100) axis. In the following, we will define angles relatively to the (110) axis corresponding to the cleaved edge of the sample. We thus introduce the new angle $\theta_s=\theta_s'-45°$.

Through the study of nonmagnetic QDs, we will discuss in the following the strained induced linear polarization anisotropy observed in single QD luminescence. We analyze then the interplay between the strain anisotropy and anisotropies due to e-h exchange in an elongated potential or an in-plane magnetic field and show that the valence-band mixing is also responsible for a significant in-plane hole g factor.

IV. VALENCE-BAND MIXING AND OPTICAL ANISOTROPY

Figure 3 presents the polarization resolved emission spectra for different charged states of the same QD (QD3): the neutral species (exciton and biexciton) and two charged excitons (positive and negative). Whatever the charged state, the emission of QD3 is partially linearly polarized along a constant direction. In this case, the linear polarization rate ρ_L equals 40%.[16] A significant linear polarization rate is ob-

served for most of the investigated QDs but with polarization directions changing from dot to dot.

To explain these polarization properties, let us consider a QD presenting an inhomogeneous distribution of strains. Because of the strained induced VBM described by the Hamiltonian (5), the general form for the lowest energy hole states is

$$|\varphi_h^{\pm}\rangle \propto \chi_{hh}(\vec{r})|\pm 3/2\rangle - \frac{w_{lh}}{w_{hh}}\chi_{lh}(\vec{r})|\mp 1/2\rangle, \tag{6}$$

where $w_{lh(hh)}$ is the probability for the hole to be light (heavy) and $\chi_{lh(hh)}(\vec{r})$ its envelope function. By reducing the study to the approximation of weak valence-band mixing ($\rho_s \ll \Delta_{lh}$), the ratio w_{lh}/w_{hh} can be replaced by $\rho_s/\Delta_{lh}e^{\pm 2i\theta_s}$. The polarization of the optical transitions involving these hole states is strongly perturbed by the light-hole part of the wave function. Using the optical selection rules given in Appendix B, we find that both recombinations of $|\downarrow_e, \varphi_h^+\rangle$ and $|\uparrow_e, \varphi_h^-\rangle$ e-h pairs have oscillator strengths that read as

$$\Omega(\phi) \propto 1 + A^2 + 2A\cos(2(\alpha - \theta_s)), \tag{7}$$

with

$$A = \frac{1}{\sqrt{3}}\frac{\rho_s}{\Delta_{lh}}\frac{\int \chi_e(\vec{r})\chi_{lh}(\vec{r})d\vec{r}}{\int \chi_e(\vec{r})\chi_{hh}(\vec{r})d\vec{r}}, \tag{8}$$

where ϕ is the angle between a linear analyzer and the (110) axis. The dot emission is then partially linearly polarized along a direction defined by θ_s with a polarization rate of $\rho_L = 2A/(1+A^2)$.

For a larger valence-band mixing, the form of Ω is more complex but the polarization direction remains the same and the polarization rate is still controlled by ρ_s/Δ_{lh}. This explanation of the observed linear polarization implies that the luminescence of the QD reflects the oscillator strength of the transitions. This is not surprising for fully spin degenerated charged excitons. For neutral species presenting a fine structure splitting, this suggests a fast exciton spin relaxation[18] or that $J_z = \pm 1$ excitons are successfully injected in the dot. In the latter case, after the injection, the excitonic state will oscillate between the eigenstates of an anisotropic QD during the coherence time of the exciton.[19] If this coherence time is not too short compared to the exciton lifetime, the PL intensity of the X and Y eigenstates will perfectly reflect their oscillator strength.

In order to estimate the values of the parameters responsible for the polarization features of QD3, we diagonalized the electron-hole spin Hamiltonian including H_{BP} and calculated the optical transitions oscillator strengths. In the calculation of the charged excitons transitions, the only adjustable parameters are ρ_s/Δ_{lh}, θ_s, and the ratio of the e-lh and e-hh overlap integrals defined in Eq. (8).

We have no direct information about the value of the e-lh and e-hh overlap integrals but we can do some assumptions about their ratio: First, the behavior of excitons in CdTe/ZnTe QDs shows that holes are mainly heavy. Thus, the probability ratio w_{lh}/w_{hh} defined in Eq. (6) cannot be larger than 1. For the extreme case $w_{lh}/w_{hh}=1$, the ratio of the e-lh and e-hh overlap must be roughly equal to 0.5 to reproduce the measured polarization rate. This large value of the overlap ratio shows that light holes have to be well confined in the QDs. Nevertheless, it is unlikely for the light holes to be more confined than heavy holes. It follows that the overlap ratio must lie between 0.5 and 1. In the following calculation, we will consider an overlap ratio equal to 0.8. Due to this assumption, the model we developed allows only a qualitative description of the influence of the VBM.

In this framework, the polarization rate and the direction of polarization measured for the QD presented in Fig. 3 can be reproduced with $\rho_s/\Delta_{lh}=0.75$ and $\theta_s=10°$ [Fig. 4(b)]. This numerical estimation shows first that the approximation of weak valence-band mixing used in Ref. 3 is no longer valid for a system presenting a polarization rate of about 40%. On the contrary, the valence-band mixing is quite strong leading to a light-hole probability in the ground state of about 25%. This significant value of ρ_s/Δ_{lh} may be explained by a smaller splitting between the light and heavy holes than expected. As a matter of fact, biaxial strains in the studied QDs are partially relaxed. Moreover, it has also been proposed recently that light holes could be confined at the dot interfaces due to the inhomogeneous strain distribution, increasing the hh-lh mixing.[20]

Let us consider now in more detail the emission of QD3 exciton (see Fig. 3). It presents a linearly polarized doublet with a splitting of about 200 μeV. As expected, the line intensities are modulated by the strain-induced polarization of the dot. Nevertheless, one also notes that these two lines are not perpendicular to each other but form an angle χ_X of about 110°. Because of the long range part of the e-h exchange interaction, the two lines of X are expected to be polarized parallel and perpendicular to the axis defined by the dot in-plane shape. Because of the local distortion of the CdTe layer, the shape anisotropy axis is not necessarily identical to the strain axis. An angle between these two axes will lead to a competition between strains and dot shape to control the polarization anisotropy of the dot.

To describe the polarization properties of the neutral exciton, we have to solve the full spin Hamiltonian including the e-h exchange interaction (long range and short range) and the strain effects described by the Hamiltonian (5). In confined systems, the short range part of e-h exchange interaction strongly depends on the overlaps between electrons and holes.[21] A detailed description of the short range exchange integrals and of the e-h overlap integrals used in these calculations are presented in Appendixes C and D. To fully describe the polarization properties of the neutral exciton, five energy parameters must be known or adjusted: ρ_s, Δ_{lh}, the long-range (δ_0^{lr}) and short-range (δ_0^{sr}) parts of the energy splitting between the bright and dark excitons, and the long-range exchange energy δ_2.

The contribution of the long range exchange interaction to the bright-dark splitting in quantum dots is still controversial. Some theoretical publications predict it to be comparable to the short range one and even greater in nanocrystals.[22–24] In our system, we will consider that the splitting between dark and bright excitons is equally divided between δ_0^{lr} and δ_0^{sr}.

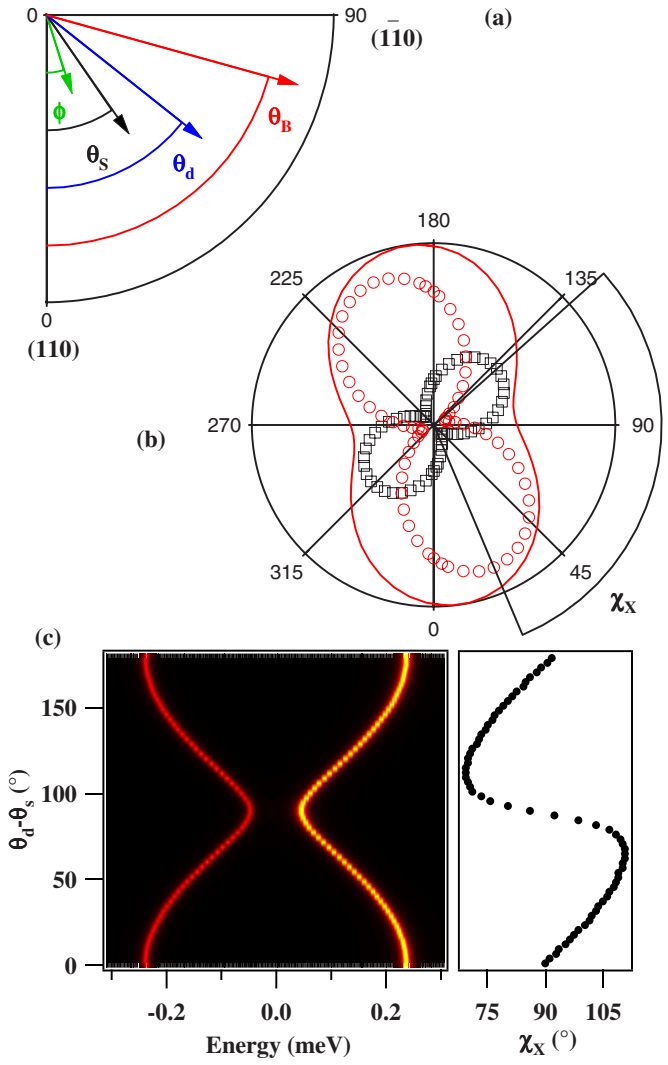

FIG. 4. (Color online) (a) Scheme of the angle definitions used in the discussion. The angles $\theta_{s,d,B}$ are, respectively, the strain, dot shape, and in-plane magnetic field orientation. The analyzer direction is given by ϕ. (b) Calculated polar plots of the emission intensities of the low energy line (square), high energy line (circle), and overall polarization anisotropy (solid line) of X obtained with a model including both the valence-band mixing and the e-h exchange interaction. The set of parameters used for the calculation is $\Delta_{lh}=30$ meV, $\rho_s/\Delta_{lh}=0.75$, $\theta_s=10°$, $\delta_0^{sr}=\delta_0^{lr}=400$ μeV, $\delta_2=250$ μeV, and $\theta_d-\theta_s=70°$. (c) Simulation of the evolution of radiative doublet splitting and of the angle χ_X when varying the angle $\theta_d-\theta_s$ between the strain direction and the dot-shape direction.

For QD3, the splitting δ_0 can be extracted from the magneto-optical measurements and is around 800 μeV. The value of δ_2 is strongly dependent on the dot geometry and values up to 500 μeV have been measured in II-VI quantum dots.[25]

We can hardly access experimentally to the parameters ρ_s and Δ_{lh} separately. The only information available is that, in PLE measurements, the first excited states of the dots (except phonon replica) lie around 30 meV above the ground state. This gives a minimal value for Δ_{lh}. However, the absolute values of ρ_s and Δ_{lh} have no effects on the splitting of the radiative ground state. Indeed, the coupling due to the short range exchange interaction between "mainly heavy" and "mainly light" excitons, separated by Δ_{lh}, is negligible. The only significant coupling caused by the combined effect of the exchange interaction and the VBM occurs between the two mainly heavy bright excitons: a hh-lh mixing, as described in Eq. (6), allows simultaneous electron-hole spin flips. Consequently, the two radiative excitons states are split into two linearly polarized lines by the short range exchange interaction. The value of this splitting is controlled by δ_0^{sr} and by the probabilities w_{lh} and w_{hh} depending only on the ratio ρ_s/Δ_{lh}. The linear polarization directions are then determined by the strain direction θ_s. Thus, the competition between the dot-shape and the strain distribution cannot be reduced to the modulation of two linearly polarized lines depending on the dot geometry by an envelope defined by the strain anisotropy. There is an interplay between two similar effects acting on the bright exciton states, each of them trying to impose a given direction for the polarization of the radiative doublet.

In order to extract the main parameters controlling this interplay, we carried out a simulation yielding the radiative splitting and the angle χ_X between the two polarized exciton lines as a function of the angle between the strain direction and the dot-shape direction. Figure 4(c) gives the associated results. The ratio ρ_s/Δ_{lh} has been chosen equal to 0.75 to reproduce the polarization rate of QD3. The strain direction θ_s is fixed at 10° while varying the direction of the dot shape θ_d. δ_0^{lr} and δ_0^{sr} are both equal to 400 μeV. δ_2 remains an adjustable parameter. We will see later that it must be around 250 μeV to properly reproduce the polarization properties of QD3 [Fig. 4(b)].

We observe in the calculation presented in Fig. 4(c) that both the splitting of the lines and their direction of polarization are very sensitive to the angle $\theta_d-\theta_s$ between the strain direction and the dot direction. The splitting varies between 100 and 500 μeV. It is maximal when the dot and the strain directions are parallel and minimal when they are perpendicular. One can compare two extreme cases to understand this variation. When the splitting of the radiative lines is mainly caused by the combined actions of the short range exchange interaction and of the valence-band mixing, the VBM-induced splitting is modulated by a sinusoidal perturbation with an amplitude defined by the long range exchange energy δ_2. In this case, the dot geometry has only a weak influence on the polarization directions and the high energy line presents the largest intensity. On the opposite, when the long range exchange splitting is larger than the VBM-induced splitting, the situation is reversed and the exchange-induced splitting is slightly perturbed by the VBM. The dot geometry has then a strong influence on the polarization. Even if the overall linear polarization of the structure is defined by the valence-band mixing, the intensity is mainly found on the high energy line if the strain and dot direction are parallel and on the low energy line if they are perpendicular.

On the right panel of Fig. 4(c), the behavior of the polarization directions seems more complex: The polarization directions are orthogonal when the dot direction is parallel or perpendicular to the strain direction but one can observe a deviation of ±20° from this usual behavior when the angle

$\theta_d - \theta_s$ is slightly acute or obtuse. The maximum deviation increases when increasing δ_2 or ρ_s/Δ_{lh}. The shape of the variation changes from a sinus in the limit cases where one of the energy parameters (short or long range) dominates the other to a diver shape [see Fig. 4(c)] when the short range and long range energies are similar.

It follows from this simulation that a possible set of parameters for the studied dot (QD3) is $\delta_2 \simeq 250$ μeV and a relative angle between strain and dot directions around 70°. Measurements on other QDs show that, in the studied samples, there is no correlation between the polarization rate of the emission and the excitonic splitting. Splittings lie between 30 and 300 μeV, while the linear polarization can reach 50%. In particular, one can find different QDs with large or small splitting but with a large linear polarization rates of about 40%. The excitonic splitting is thus in general produced by the joined action of the short range e-h exchange interaction, through the VBM, and of the long range one as detailed for QD3. It also appears that strain distribution is not correlated with the dot geometry. In average, the values of the measured valence-band mixing and anisotropic long range exchange energies are quite large, in agreement with recent calculations reported in the literature.[3,22–24] One can finally note that taking into account only the VBM due to the nondiagonal terms of the Luttinger-Kohn Hamiltonian in an anisotropic potential could not explain the observed angle between the linearly polarized exciton components. Indeed, in this case, the mixed hole states reflect the symmetry of the dot shape. The phase of the short range and long range coupling terms are identical and the linear polarization direction of the radiative doublet remains orthogonal. Even if a quantitative description of these QDs should include corrections coming from the Luttinger Hamiltonian, the main characteristic of the PL (i.e., the polarization amplitude and directions) would still be controlled by the strained induced VBM.

V. VALENCE-BAND MIXING AND MAGNETIC ANISOTROPY

To have a better understanding on the influence of the VBM on the spin properties of confined carriers, magnetic field studies were performed. A combination of data obtained for magnetic fields in Faraday and Voigt configurations [Fig. 5(a)] allows a determination of the magnetic properties of QD3. In Faraday configuration ($B \| z$), X, X^+, X^-, and X_2 split into doublets. In the heavy-hole approximation, these doublets should be composed of two lines with opposite circular polarizations $\sigma+$ and $\sigma-$. Experimentally, we only observe circular polarization rates from 75% to 85% at 11 T as illustrated in Figs. 5(d) and 5(e) for the charged excitons. This is not surprising because the magnetic field has no influence on the valence-band mixing. Considering a valence-band mixing efficiency ρ_s/Δ_{lh} of about 0.75, it appears that each line of the doublets should have elliptic polarizations with linear polarization rates of 40% and circular polarization rates of 90%. In other words, a 40% linear polarization of the QD emission is conserved whatever the charge state and whatever the magnetic field configuration. For the exciton, an anticrossing of the bright and dark exciton states is observed

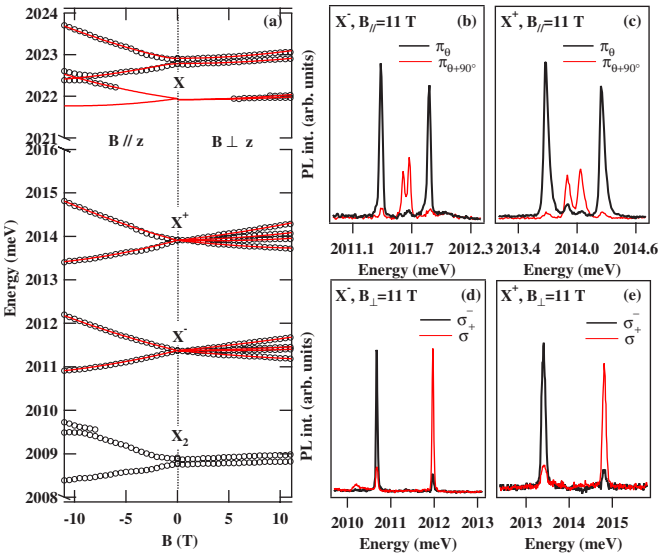

FIG. 5. (Color online) (a) Fine structure under magnetic fields of X, X^+, X^-, and X^2 of QD3 in both Voigt ($B_\perp z$) and Faraday ($B_\| z$) configurations. (b) and (c) show, respectively, the linearly polarized PL spectra of X^- and X^+ in a transverse magnetic field $B=11$ T. (d) and (e) show the circularly polarized PL spectra of X^- and X^+ in Faraday configuration ($B=11$ T). The observed different splittings directly reveal a variation of the g factor with the charged state of the QD.

around 9 T allowing a full determination of the electron and hole g factors. This anticrossing can be understood only by considering nonzero trigonal shear strains [$\epsilon_{zx(zy)}$]. In this case, the full Bir-Pikus Hamiltonian must be used and one obtains hole eigenfunctions that are linear combinations of $|3/2\rangle$, $|1/2\rangle$, and $|-1/2\rangle$ on one side and $|-3/2\rangle$, $|1/2\rangle$, and $|-1/2\rangle$ on the other side. In this new basis, the Zeeman Hamiltonian in Faraday configuration is no more diagonal. Thus, it couples these hole states producing anticrossings when they get close to each other as observed experimentally.

In Voigt configuration ($B \perp z$), the splitting of the exciton doublet slightly increases and at high field a contribution of the dark exciton states is also observed on the low energy side of the spectra (Fig. 5). By contrast, the charged excitons split into quartets of linearly polarized lines [Figs. 5(b) and 5(c)][26] with an intensity difference between the linearly polarized components corresponding to the polarization degree measured at zero field. This spectral feature is a direct consequence of the presence of the strong hh-lh mixing detailed previously. The magnetic coupling of the hole in a D_{2d} geometry is given by

$$\mathcal{H}_B^h = \mu_B g_0 [\kappa J \cdot B + q(J_x^3 B_x + J_y^3 B_y + J_z^3 B_z)]. \quad (9)$$

As it has been recently shown in CdSe QDs,[3] in the presence of hh-lh mixing, the κ term of the hole magnetic Hamiltonian leads to magnetic coupling between the hole states for $B \perp z$, resulting in a nonzero value of the in-plane hole g factor and in QD PL emission polarized parallel and perpendicular to

TABLE I. g factors extracted from the magneto-optics measurements on QD3.

	X	X^+	X^-
$g_{e\perp}$	−0.40	−0.35	−0.35
$g_{h\perp}$	0.16	0.19	0.17
$g_{e\parallel}$	−0.45	−0.45	−0.45
$g_{h\parallel}$	0.53	0.60	0.53

the QD strain axes. We will see in the following some deviation from these results in the studied QDs.

Magneto-optical experiments enable a determination of the electron and hole g factors parallel and perpendicular to the growth axis. A summary of the g factors deduced from the magnetic field evolution of the different charged states of QD3 is presented in Table I. An increase of the hole g factor is found for X^+ in both Faraday and Voigt configurations. This variation of g_h reflects the expected variation of the hole confinement in the different excitonic species. For X or X^-, a significant fraction of the confinement of the hole comes from the Coulomb attraction of the electrons present in the initial state of the optical transitions. By contrast, in the final state of X^+, there is no electron to attract the hole, resulting in a delocalization of the hole wave function in the ZnTe barrier and to a modification of its g factor.

As observed for the linearly polarized exciton doublet at zero field, the charged exciton quadruplets under transverse magnetic field present polarization axes which are not orthogonal. This can be seen in Fig. 6 where the polarization resolved spectra of charged excitons in QD3 are plotted for a transverse magnetic field $B_\perp = 11$ T. Not only the inner and outer doublet polarizations are not perpendicular to each other but there are also differences in the polarization directions of each doublet. In the first part of this article, we have seen that a competition can arise between the strain distribution and the shape of the dots that define two different anisotropy axes in the QD plane. This competition has consequences on the exciton splitting and polarization features. Thus, for magneto-optical experiments in Voigt configuration, one can expect that the spectral features of the charged exciton emission will be influenced by a competition between the strain distribution and the in-plane anisotropy produced by the magnetic field.

As illustrated in Fig. 7, we have measured the emission spectra and polarization directions of QD4 negatively charged exciton for two orientations of the in-plane magnetic field. It appears that the orientation of the magnetic field in the QD plane has a significant impact on the Zeeman splitting and on the polarization directions of the inner and outer doublets. When the in-plane magnetic field is perpendicular to the (110) axis [Fig. 7(a)], the charged exciton splitting only enables us to observe a triplet structure and the inner and outer doublets are roughly perpendicular with directions defined by the strain distribution as explained in Ref. 3. In the second case presented in Fig. 7(b) where $\theta_B = 30°$, the splitting has changed so that a quadruplet is observable. The angle $\chi_{out\text{-}in}$ between the inner and outer doublets is now only

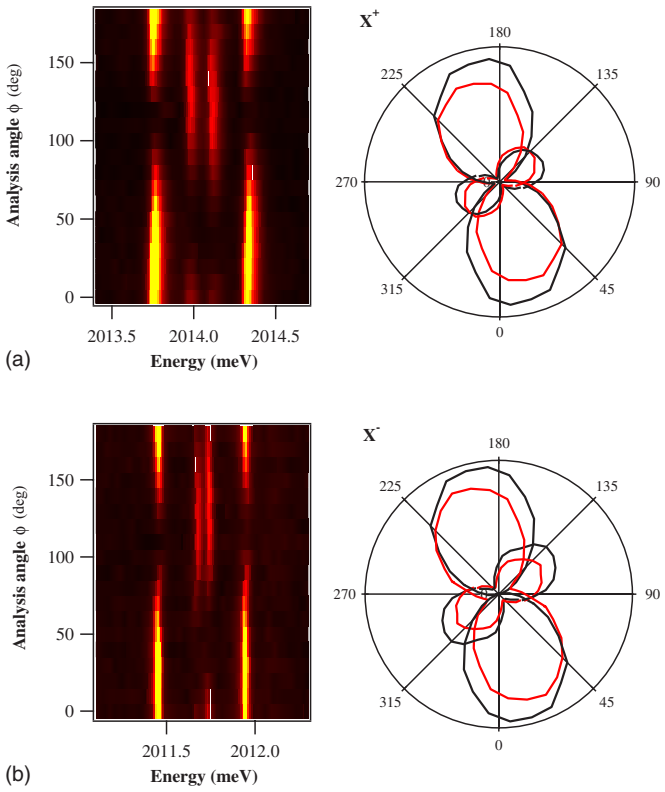

FIG. 6. (Color online) Polarization resolved fine structures of X^+ (a) and X^- (b) for QD3 polar graphs of the line intensities are plotted on the right panel. Black lines correspond to the low energy lines and red lines to the high energy lines.

70°. This confirms that the charged exciton behavior under transverse magnetic field is nontrivial. A competition between the strain anisotropy axis and the magnetic field direction governs the hole state.

Such a competition can be qualitatively modeled by considering only the linear term of $\mathcal{H}_B^h$. The calculated results presented in Fig. 8(a) show that for some magnetic field orientations, one can have either an acute or obtuse angle $\chi_{out\text{-}in}$ between the linear polarization directions of the inner and outer doublets. The angle $\chi_{out\text{-}in}$ [right panel of Fig. 8(a)] as well as the Zeeman splitting [left panel of Fig. 8(a)] present both an amplitude which strongly depends on the transverse magnetic field orientation. In particular, extremal splitting values and orthogonality of the doublet directions are obtained for magnetic field orientation parallel to the strain direction. We note that these modulations cannot be seen in the pseudospin model used for instance in Ref. 3 in which the reduction to a 2×2 matrix cancels the phase of the coupling elements. Figure 8(b) shows that sharing the hole g factor between the linear and the cubic components ($q \neq 0$) modifies the splitting and angle variations. In particular, we observe an angular shift of the modulation shapes. However, a comparison with the experimental data does not permit to independently extract the values of κ and q. They may both contribute to the observed behavior. The presented model is also not able to reproduce the dephasing between the two inner lines on one side and the two outer lines on the other side. In order to improve the model, the g factor anisotropy

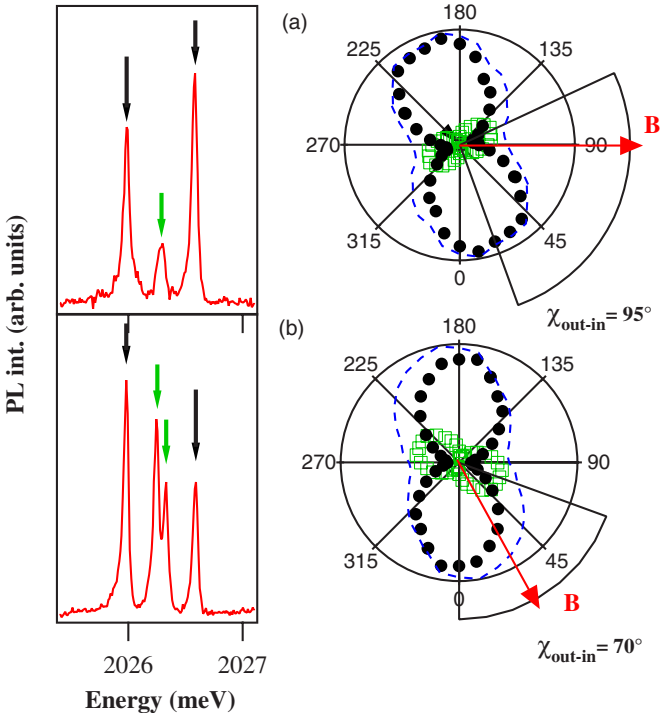

FIG. 7. (Color online) Fine structures and polar graphs of the emission intensity of QD4 negatively charged exciton for two orientations of the transverse magnetic field (11 T): (a) $\theta_B=90°$ and (b) $\theta_B=30°$ while $\theta_s=10°$ in both cases. In the polar graphs, the intensity of the inner doublet is plotted with open green squares. The intensity of the outer doublet is plotted with full black circles. The dashed blue lines represent the total emission intensity.

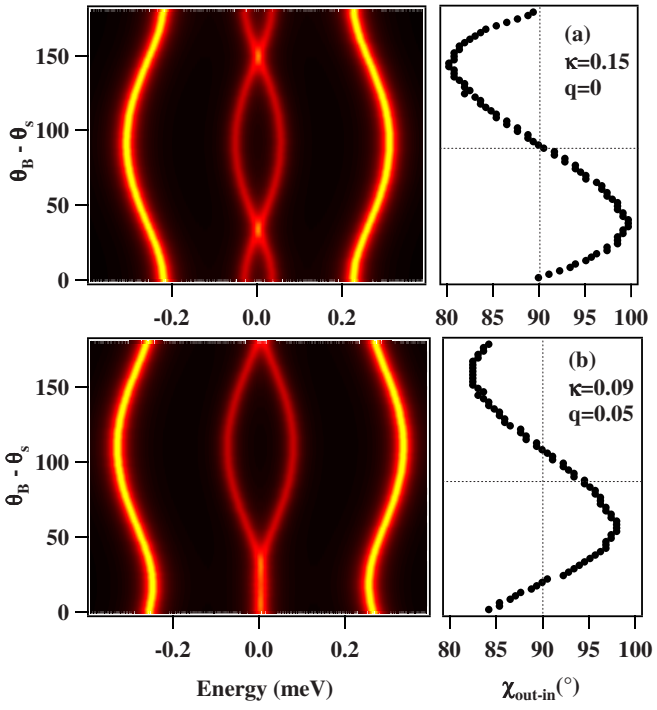

FIG. 8. (Color online) Calculated dependence of the fine structure and of $\chi_{out\text{-}in}$ on the magnetic field direction θ_B for two different sets of parameters: (a) $\kappa=0.15$, $q=0$; (b) $\kappa=0.09$, $q=0.05$. These parameters are chosen to reflect the experimental in-plane hole g factor. The strain parameters are still $\Delta_{lh}=30$ meV, $\rho_s/\Delta_{lh}=0.75$, and $\theta_s=10°$.

due to the shape of the confinement and VBM due to Luttinger Hamiltonian should probably be considered.

VI. VALENCE-BAND MIXING IN MAGNETIC QUANTUM DOTS

Considering now single Mn-doped QDs, the *sp-d* exchange interactions between the confined carriers and the single Mn atom are responsible for a peculiar fine structure of the emission.[1] It has been demonstrated that the hole-Mn spin interaction is of prime importance in this fine structure, because of its energy range and above all because of the spin anisotropy of the hole.[27,28] It appears clearly that a valence-band mixing will have dramatic consequences on the emission fine structures of an exciton coupled with a single Mn atom. In the heavy-hole approximation, a hole acts on the Mn spin as an effective magnetic field applied along the growth axis, lifting its spin degeneracy. If a mixing of heavy and light holes is introduced, one has to consider a system of coupled spins in which hole-Mn spin flips are possible.

To understand the effects of this change, we first consider the emission of the negatively charged exciton in a single Mn-doped quantum dot [Fig. 9(c)]. In the final state of the X^- optical recombination, the system is composed of a single Mn atom interacting with the resident electron. The exchange interaction between them is isotropic so that we can consider a $J=5/2+1/2=3$ spin system. It is composed of two energy levels. The lower energy level is the parallel spin configuration ($J=3$). It is sevenfold degenerated. The upper energy level ($J=2$) is fivefold degenerated. When an electron-hole pair is injected in the dot, the excitonic state is composed of two spin-paired electrons, one hole and the Mn atom. The system is governed by the hole-Mn exchange interaction. Figure 9(a) presents the influence of an increasing valence-band mixing, characterized by ρ_s/Δ_{lh}, on the energy structure of the hole-Mn complex. The heavy-hole–light-hole splitting due to biaxial strains Δ_{lh} is maintained equal to 30 meV. The hole-Mn exchange integral $I_{h\text{-}\mathrm{Mn}}$ is set to 170 μeV as estimated in previous work[28] and the values of wave function overlap integrals are still those given in Appendix D.

It is not possible to extract from the experiment the position of the Mn atom inside the dot and thus to estimate overlaps between the Mn atom and the confined carriers. In our calculation, the exchange integrals are then effective parameters and identical hh-Mn and lh-Mn overlaps are considered. In the plot presented in Fig. 9(a) the origin of the energy is chosen at the barycenter of the hh-Mn energy levels. At zero valence-band mixing, there are six hh-Mn energy levels. For each heavy-hole spin ($\pm 3/2$), the levels are associated with the six Mn spin projections ($S_z=5/2\cdots-5/2$). Due to the antiferromagnetic hh-Mn exchange interaction, the antiparallel spin configurations ($|3/2_h,-5/2_{\mathrm{Mn}}\rangle$ and $|-3/2_h,5/2_{\mathrm{Mn}}\rangle$) are stabilized.

When increasing the value of ρ_s/Δ_{lh}, we observe that the energy levels gather into two sets. The upper energy set is

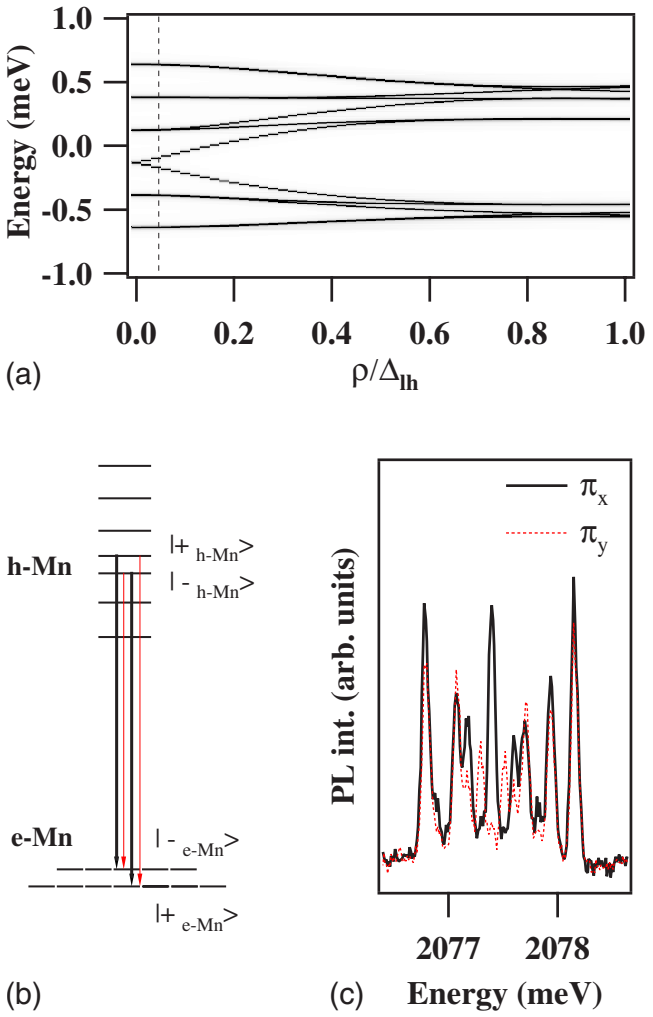

FIG. 9. (Color online) (a) Dependence of the hole-Mn energy spectrum on the strength of the valence-band mixing ρ/Δ_{lh}. The dotted line corresponds to the situation described in the scheme (b) and associated with QD5 (c) (ρ/Δ_{lh}=0.05). (b) Scheme of the polarized transitions of the negatively charge exciton in a single Mn-doped QD. The axes, x and y do not correspond here to the crystallographic axes. (c) Polarization resolved photoluminescence of the negatively charged exciton of QD5.

composed of seven states and the lower one of five. In a first approximation, the situation becomes similar to the electron-Mn case. The hole spin looks like an isotropic pseudospin 1/2 but it is not: As shown in Fig. 9, at high values of ρ_s/Δ_{lh}, there is still a fine structure in both level sets. Moreover, several splittings appear at ρ_s/Δ_{lh}=0.2 and 0.5, which should not exist when considering a simple pseudospins 1/2. This originates from the existence of the upper energy hole states (light holes), shifted 30 meV above by the biaxial strains. Because of this splitting, the valence-band mixing cannot turn the hole-Mn interaction into an isotropic interaction between the Mn spin and a pseudospin 1/2. One also notes a decrease of the overall splitting of the energy spectrum. This shows the decrease of the heavy-hole statistical weight w_{hh} in the hole wave function as ρ_s/Δ_{lh} increases.[29,30]

One of the main effects of the VBM on the h-Mn energy spectrum is the splitting of the third lower energy level at low values of ρ/Δ_{lh}. In the absence of VBM, this state is twofold degenerated and corresponds to the hole and Mn spin projections $|3/2_h,-1/2_{\mathrm{Mn}}\rangle$ and $|-3/2_h,1/2_{\mathrm{Mn}}\rangle$. But as soon as a weak VBM is introduced, the hole spin states must be described by Eq. (6). The hole can now flip its spin with the Mn atom coupling the heavy part of a φ_h state to the light part of the other. The two resulting h-Mn eigenstates are

$$|-\rangle_{h\text{-Mn}} = \frac{1}{\sqrt{2}}(|\varphi_h^+,-1/2_{\mathrm{Mn}}\rangle - |\varphi_h^-,1/2_{\mathrm{Mn}}\rangle), \tag{10}$$

and

$$|+\rangle_{h\text{-Mn}} = \frac{1}{\sqrt{2}}(|\varphi_h^+,-1/2_{\mathrm{Mn}}\rangle + |\varphi_h^-,1/2_{\mathrm{Mn}}\rangle). \tag{11}$$

These bounding and antibounding states can either recombine on the electron-Mn states,

$$|-\rangle_{e\text{-Mn}} = |20\rangle_{e\text{-Mn}} = \frac{1}{\sqrt{2}}(|\uparrow_e,-1/2_{\mathrm{Mn}}\rangle - |\downarrow_e,1/2_{\mathrm{Mn}}\rangle), \tag{12}$$

or

$$|+\rangle_{e\text{-Mn}} = |30\rangle_{e\text{-Mn}} = \frac{1}{\sqrt{2}}(|\uparrow_e,-1/2_{\mathrm{Mn}}\rangle + |\downarrow_e,1/2_{\mathrm{Mn}}\rangle), \tag{13}$$

producing four linearly polarized emission lines [see Fig. 9(b)]. The polarization directions are only defined here by the strain-induced coupling so that two of the four lines are parallel to the strain direction and the others are perpendicular to it. This effect can be observed in the emission spectrum of the negatively charged exciton of QD3 [Fig. 9(c)]. Two π_y polarized lines and an intense π_x polarized line lie on the center of the fine structure.[28] Despite a weak valence-band mixing (a value of ρ_s/Δ_{lh}=0.05 is used to reproduce the spectrum of QD5), as the unperturbed states are degenerated, the hole-Mn spin flips significantly influence the emission feature of the charged Mn-doped QDs.

One can also find a signature of the valence-band mixing in the emission spectra of neutral single Mn-doped QDs. In a Mn-doped QD, the ground state of the exciton is composed of six bright energy levels and six dark energy levels resulting from the coupling of bright excitons and dark excitons with the six projections of the Mn spin. For a given exciton spin (±1 or ±2), the six Mn spin projections have different energies. In this system, the hole spin interacts with both the Mn spin and the electron spin. The effect of an increasing valence-band mixing on the excitonic emission spectrum of a QD is presented on Fig. 10(a). Parameters are chosen to reproduce the features of QD5 emission spectrum plotted on Fig. 10(b): The e-Mn exchange integral $I_{e\text{-Mn}}$ is set to 70 μeV; the splitting between the bright and dark excitons δ_0 is chosen equal to 550 μeV, equally divided among the long range and short range e-h exchange interaction. Other parameters are the same than in the previous charged exciton calculation.

Let us first consider the influence of the electron-hole exchange interaction. We have seen in the case of nonmagnetic

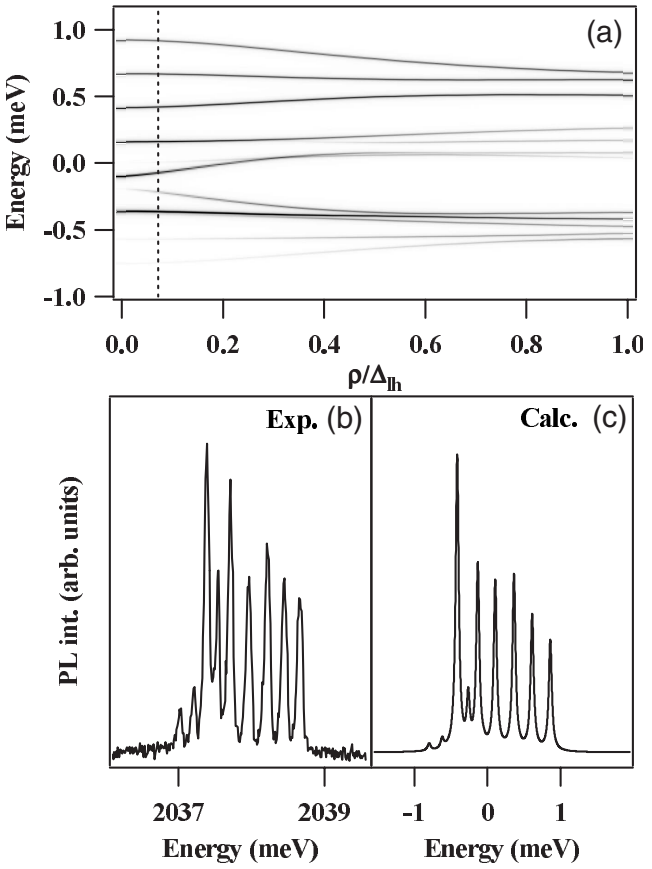

FIG. 10. (a) Dependence of the exciton-Mn energy spectrum on the strength of the valence-band mixing ρ/Δ_{lh}. The dotted line corresponds to the situation of QD6 ($\rho/\Delta_{lh}=0.07$). (b) and (c) are the experimental and calculated emission spectra of QD6.

QDs that, in first approximation, the only effect of the valence-band mixing on the short range e-h exchange is to couple bright exciton states together. For magnetic QDs, bright states associated with the same Mn spin projection are thus coupled. This coupling mainly concerns the energy levels associated with Mn spin projections $\pm 1/2$ only slightly split by the exciton-Mn exchange interaction. An increase of the valence-band mixing will thus open a slight gap in the middle of the bright exciton fine structure [around 0.25 meV in Fig. 10(a)].

Another gap appears on the low energy side of the structure because of the hole-Mn interaction. As a matter of fact, simultaneous hole-Mn spin flips couple bright and dark states associated with consecutive Mn spin projections. The exciton-Mn exchange interaction induces an overlap of the bright and dark exciton fine structures. States coupled by h-Mn spin flips are therefore quite close to each other and an increase of the VBM, that is to say an increase of the h-Mn spin flip efficiency, will open a gap between them. This can be observed on Fig. 10(a) around −0.1 meV. Finally one may note once again that the overall splitting of the structure decreases as the VBM increases because of the decrease of the weight of the heavy hole in the exciton ground state.

Such coupling between the bright and dark excitons is observed in the spectrum of QD6 presented in Fig. 10(b). In this QD, the valence-band mixing is quite weak and the gaps induced by the e-h exchange and the h-Mn exchange can be hardly resolved in the exciton spectrum [Fig. 10(b)]. Nevertheless, the h-Mn spin flip-induced bright-dark coupling is large enough to give non-negligible oscillator strengths to the dark states. Three "dark" states are then observed in the emission spectrum. The value ρ_s/Δ_{lh} can be estimated to 0.07. Using this parameter, we can calculate QD6 exciton emission spectrum. The result is plotted on Fig. 10(c). It has been shown in previous work[1] that the exciton-Mn system is partially thermalized during the exciton lifetime. This results in the increase of the intensity of the lines as their energy decreases. In the calculation, we thus consider that the system has relaxed and that it is characterized by an effective spin temperature T_{eff} depending both on the phonon bath and on the hot carrier gas produced by the laser excitation. In Fig. 10(c), $T_{eff}=15$ K. With this effective temperature, dark states appear in the calculated spectrum but their intensity is weaker than in the experiment. Moreover, comparing the intensities of the bright lines in the calculation and in the experiment, we note that we cannot fit the data with an effective temperature smaller than 15 K in order to increase the dark state intensity. These features show that we should not consider a total thermalization in the exciton-Mn system: If the spin relaxation is partially blocked, it is difficult to thermalize the system. As bright and dark excitons are created with the same generation rate, the intensities of the associated transitions can be comparable even though they have different oscillator strengths. This is particularly the case under weak excitation conditions where the influence of the hot carrier gas spin reservoir is reduced.

We finally consider the neutral exciton fine structure of a single Mn-doped QD that presents an anisotropic in-plane shape (QD7 presented in Fig. 11). Effects of the long range electron-hole exchange interaction on the emission spectrum of a single Mn-doped QD were discussed in a former letter.[31] Nevertheless, details of the polarization properties were not analyzed. Here, we detail these polarization features and show that the VBM is once again necessary to explain them. Figure 11 presents the linear polarization dependence of the emission spectrum of QD7. The experimental spectrum shows the main characteristics of a quite strong VBM as detailed in Fig. 10(a). The spectrum presents an overall linear polarization rate of about 25% orientated at $\theta_s=110°$ from the cleaved edge of the sample and dark states appear on the low energy side of the structure. Two gaps can also be observed: One between the two first main lines and the other between the third and the fourth lines. However, if these peculiarities were only due to the combined effect of the VBM and short range e-h exchange, one could expect the third and the fourth lines to be polarized parallel and perpendicular to the strain direction (110°). It is not the case and surprisingly, the emission spectrum also presents nonorthogonal linear polarization directions.

These polarization directions are the signature of a competition between a valence-band mixing and long range electron-hole exchange interaction. The calculation of the emission spectrum of QD7 (right panel of Fig. 11) gives a good agreement with the experiment using the following parameters: $I_{e\text{-Mn}}=60$ μeV, $I_{h\text{-Mn}}=135$ μeV, $\delta_0^{lr}=\delta_0^{sr}=300$ μeV, $\delta_2=450$ μeV, $\Delta_{lh}=30$ meV, $\rho_s/\Delta_{lh}=0.25$, and

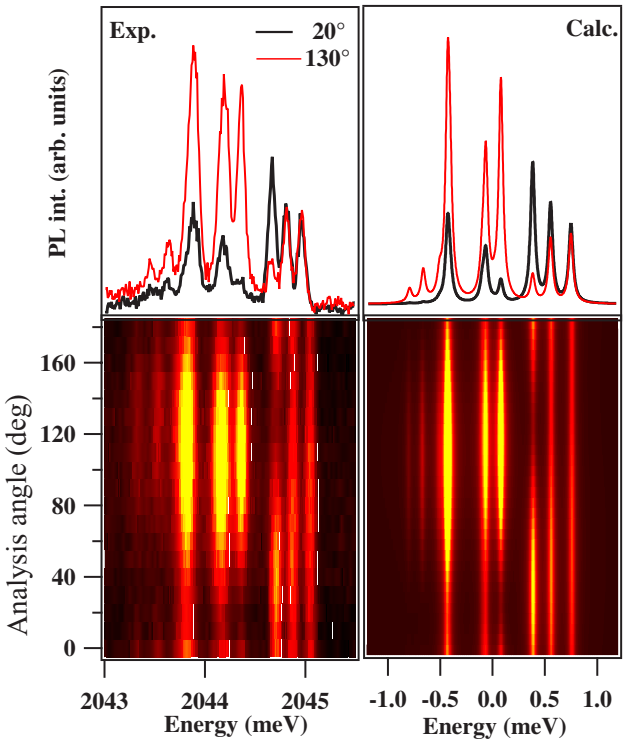

FIG. 11. (Color online) Experimental and calculated polarization resolved photoluminescence of QD6. The intensity maps present the dependence of the emission on the analyzer angle. The emission spectrum is presented for orthogonal linear analyzer directions (red and black curves).

T_{eff}=20 K. The strain direction and the dot-shape direction must be roughly perpendicular (80°) to fit the experiment. The main features of QD7 emission are well reproduced as presented in Fig. 11.

We can analyze in more detail the polarization directions of the lines by studying the polar graphs of the intensities of the six main lines (Fig. 12). We observe on the experimental graphs that the three low energy lines are mainly linearly polarized along the strain direction θ_s=110°. The third and the fourth lines have a polarization rate close to 1. This originates from the influence of the long range electron-hole exchange interaction which is maximum for these two lines. There is no significant change in the polarization directions of the three low energy lines. On the contrary, polarization directions of the three high energy lines are different. The calculation gives the same qualitative results. Actually, for the high energy lines, the influence of the long range e-h exchange decreases from the fourth to the sixth line, whereas the strain-induced polarization acts upon all the lines with an equal efficiency. Therefore, the polarization direction goes from the dot-shape direction for the fourth line to the strain direction for the sixth line. The situation is different for the three low energy lines for which the initial direction (dot-shape direction+90°) and final one (strain direction) are roughly merged. We note that we do not obtain a quantitative agreement between the experimental and the calculated linear polarization directions. In the experiments, we observe a rotation of the direction of about 30° between each line,

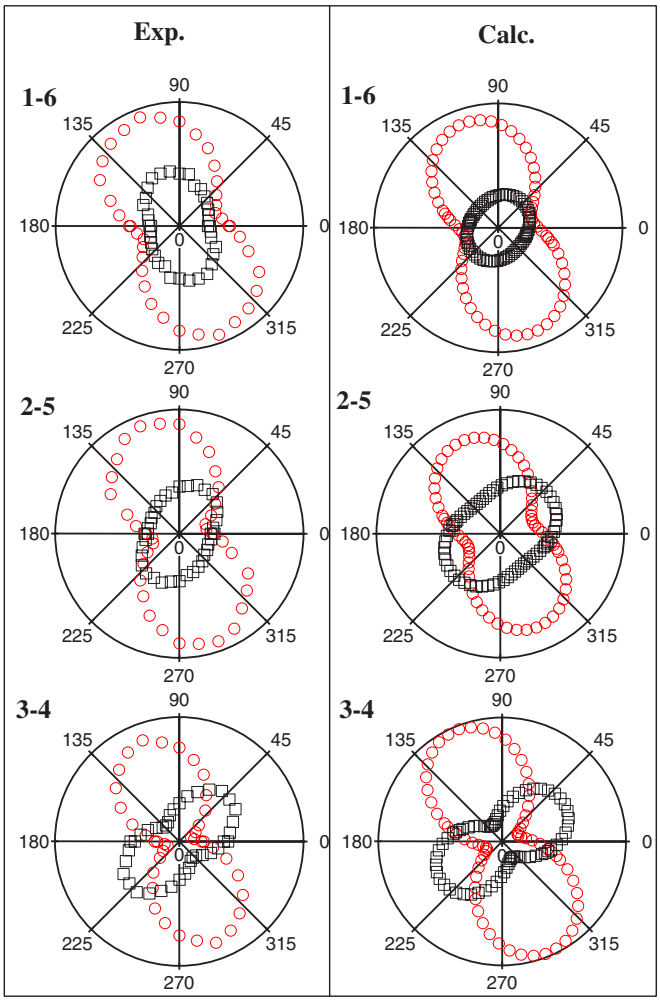

FIG. 12. (Color online) Experimental and calculated polar graphs of the intensities of the main emission lines observed in QD7. The lines are labeled by increasing energy order. In each polar graph, we compare the directions of two lines associated with the same Mn spin projection. The low energy line is plotted with red circles and the high energy one with black squares.

whereas it is only 10° in the calculation. Other origins of valence-band mixing such as confinement effects or other kinds of deformations of the lattice may play a role in these phenomena.

VII. CONCLUSION

In conclusion, we have analyzed in detail the influence of the heavy-hole–light-hole mixing on the optical fine structures of various excitonic species in single quantum dots. We have first demonstrated the controlled generation of neutral, negatively charged, and positively charged excitons in the same II-VI QD by combining a gate voltage and a photodepletion mechanism. The identification of charged excitons is supported by magnetic field studies. The strong degree of linear polarization observed for both neutral and charged species and the nonorthogonality of the linear polarization directions are explained by a combination of VBM and anisotropic e-h exchange interaction. These results show the

simultaneous influence of the anisotropic shape and anisotropic relaxation of strain in an individual quantum dot. A careful analysis of the linear polarization in transverse magnetic field shows that both the magnetic field direction and the hh-lh mixing are controlling the linear polarization directions. The valence-band mixing has also important effects in magnetic QDs. The hole cannot be considered anymore as an effective magnetic field fixed along the growth axis. Spin flips can occur with the magnetic ion, producing characteristic spectral features in the emission of neutral and charged states of the QD.

APPENDIX A: ANGULAR MOMENTUM OPERATOR

Here are written the matrices j_i of the angular momentum operator $\vec{j}$ for $j=3/2$ as described by Messiah[32] and used in this article,

$$j_x = \begin{pmatrix} 0 & \sqrt{3}/2 & 0 & 0 \\ \sqrt{3}/2 & 0 & 1 & 0 \\ 0 & 1 & 0 & \sqrt{3}/2 \\ 0 & 0 & \sqrt{3}/2 & 0 \end{pmatrix}, \tag{A1}$$

$$j_y = \begin{pmatrix} 0 & -i\sqrt{3}/2 & 0 & 0 \\ i\sqrt{3}/2 & 0 & -i & 0 \\ 0 & i & 0 & -i\sqrt{3}/2 \\ 0 & 0 & i\sqrt{3}/2 & 0 \end{pmatrix}, \tag{A2}$$

$$j_z = \begin{pmatrix} 3/2 & 0 & 0 & 0 \\ 0 & 1/2 & 0 & 0 \\ 0 & 0 & -1/2 & 0 \\ 0 & 0 & 0 & -3/2 \end{pmatrix}, \tag{A3}$$

APPENDIX B: OPTICAL TRANSITIONS

In order to obtained oscillator strength of transitions, one has to estimate the square of the dipole matrix element:[33]

$$\Omega(\vec{e}) \propto |\langle f|\vec{e}\,.\,\vec{p}|i\rangle|^2, \tag{B1}$$

where $\vec{e}$ is the observation unit vector, $|i\rangle$ and $|f\rangle$ the initial and final states, and $\vec{p}$ the kinetic momentum operator. Here, the initial state is an electron hole pair $|\chi_e(\vec{r})\psi_e\rangle|\chi_h(\vec{r})\psi_h\rangle$ ($\psi_e=\uparrow$, $\downarrow$ and $\psi_h=\pm 3/2, \pm 1/2$) and the final state is the empty state $|\varnothing\rangle$. $\Omega(\vec{e})$ is thus proportional to an overlap integral, $\int \chi_e(\vec{r})\chi_h(\vec{r})d\vec{r}$, and to one of the matrix elements of the momentum operator. The nonzero matrix elements are

$$\langle \varnothing|p_+|\uparrow 1/2\rangle = -1/\sqrt{3},$$

$$\langle \varnothing|p_+|\downarrow 3/2\rangle = 1,$$

$$\langle \varnothing|p_-|\downarrow -3/2\rangle = 1,$$

$$\langle \varnothing|p_-|\downarrow -1/2\rangle = -1/\sqrt{3}. \tag{B2}$$

APPENDIX C: ELECTRON-HOLE EXCHANGE INTERACTION

Works of Chen *et al.*[21] proposed a description of the short range e-h exchange interaction in quantum wells taking into account the different overlaps between electrons and holes. This can be summarized as follows:

$$H_{eh}^{sr} = \frac{-2\delta_0^{sr}}{3\alpha_{3/2,3/2}} \sum_{m,n} \alpha_{m,n} j_{m,n} \sigma_{m-n}, \tag{C1}$$

where

$$\alpha_{\pm 3/2,\pm 3/2} = \int (\chi_e(\vec{r})\chi_{hh}(\vec{r}))^2 d\vec{r},$$

$$\alpha_{\pm 1/2,\pm 1/2} = 2\alpha_{\pm 1/2,\mp 1/2} = \int (\chi_e(\vec{r})\chi_{lh}(\vec{r}))^2 d\vec{r},$$

$$2\alpha_{\pm 3/2,\pm 1/2} = 2\alpha_{\pm 1/2,\pm 3/2} = \int \chi_e^2(\vec{r})\chi_{lh}(\vec{r})\chi_{hh}(\vec{r})d\vec{r}.$$

Here, the spin operators are written using these notations: the electron spin notations are $\sigma_{0,1,-1}=\sigma_{z,+,-}$, and for the hole spin operator $j_{m,n}$, m and n are, respectively, the initial and final spin projections. $j_{m,n}=j_z$ when $m=n$. The energy parameter δ_0^{sr} is the short-range part of the experimental splitting between the bright and dark states.

APPENDIX D: WAVE FUNCTION OVERLAP

The wave function overlaps involved in the oscillator strength and in the electron-hole exchange can be quickly estimated using a calculation of the envelope functions for electrons, and heavy and light holes in a zero-dimensional confinement potential. We consider QDs with cylindrical symmetry. We can decouple the motion along z and in the x-y plane and solve the z and ρ Hamiltonian separately using Runge-Kutta method. A Gaussian potential is used for z and the in-plane confinement. The characteristic lengths of the radial and z confinement potential are 10 and 2.5 nm, respectively. These values are in good agreement with transmission electron microscopy characterization. One usually considers that only the electron is strongly confined in CdTe/ZnTe QDs so that we choose a depth of 700 meV for the electron well (90% of the band gap difference). Depths of the wells for the heavy and light holes are adjusted to provide an exciton overlap ratio [involved in Eq. (8)] around 0.8 and a heavy-light hole splitting Δ_{lh} around 30 meV (potential depth for heavy holes: 50 meV; potential depth for light holes: 35 meV). We use the effective masses given by Long *et al.*[34] We find the following values for the overlap integrals:

$$\frac{\int \chi_e(\vec{r})\chi_{lh}(\vec{r})d\vec{r}}{\int \chi_e(\vec{r})\chi_{hh}(\vec{r})d\vec{r}} = 0.8, \tag{D1}$$

$$\frac{\alpha_{1/2,1/2}}{\alpha_{3/2,3/2}} = 0.5, \tag{D2}$$

$$\frac{\alpha_{3/2,1/2}}{\alpha_{3/2,3/2}} = 0.7. \tag{D3}$$

[1] L. Besombes, Y. Léger, L. Maingault, D. Ferrand, H. Mariette, and J. Cibert, Phys. Rev. Lett. **93**, 207403 (2004).

[2] M. Bayer, A. Kuther, A. Forchel, A. Gorbunov, V. B. Timofeev, F. Schafer, J. P. Reithmaier, T. L. Reinecke, and S. N. Walck, Phys. Rev. Lett. **82**, 1748 (1999).

[3] A. V. Koudinov, I. A. Akimov, Yu. G. Kusrayev, and F. Henneberger, Phys. Rev. B **70**, 241305(R) (2004).

[4] F. Tinjod, B. Gilles, S. Moehl, K. Kheng, and H. Mariette, Appl. Phys. Lett. **82**, 4340 (2003).

[5] L. Besombes, Y. Léger, L. Maingault, D. Ferrand, C. Bougerol, H. Mariette, and J. Cibert, Acta Phys. Pol. A **108**, 527 (2005).

[6] L. Maingault, L. Besombes, Y. Léger, and H. Mariette, Appl. Phys. Lett. **89**, 193106 (2006).

[7] S. Bhunia and D. N. Bose, J. Appl. Phys. **87**, 2931 (2000).

[8] W. Maslana, P. Kossacki, M. Bertolini, H. Boukari, D. Ferrand, S. Tatarenko, J. Cibert, and J. A. Gaj, Appl. Phys. Lett. **82**, 1875 (2003).

[9] J. Seufert, M. Rambach, G. Bacher, A. Forchel, T. Passov, and D. Hommel, Appl. Phys. Lett. **82**, 3946 (2003).

[10] A. Vasanelli, R. Ferreira, and G. Bastard, Phys. Rev. Lett. **89**, 216804 (2002).

[11] A. Hartmann, Y. Ducommun, E. Kapon, U. Hohenester, and E. Molinari, Phys. Rev. Lett. **84**, 5648 (2000).

[12] U. Bockelmann and G. Bastard, Phys. Rev. B **45**, 1688 (1992).

[13] T. Tanaka, J. Singh, Y. Arakawa, and P. Bhattacharya, Appl. Phys. Lett. **62**, 756 (1993).

[14] S. Cortez, O. Krebs, and P. Voisin, J. Vac. Sci. Technol. B **18**, 2232 (2000).

[15] J. Allègre, B. Gil, J. Calatayud, and H. Mathieu, J. Cryst. Growth **101**, 603 (1990).

[16] This linear polarization is not due to the aperture shape in our experiment (Ref. 17). As a matter of fact, it is quite ordinary to find in the same aperture two emission lines, linearly polarized along two different directions.

[17] R. Gordon, A. G. Brolo, A. McKinnon, A. Rajora, B. Leathem, and K. L. Kavanagh, Phys. Rev. Lett. **92**, 037401 (2004).

[18] I. Favero, G. Cassabois, C. Voisin, C. Delalande, Ph. Roussignol, R. Ferreira, C. Couteau, J. P. Poizat, and J. M. Gérard, Phys. Rev. B **71**, 233304 (2005).

[19] T. Flissikowski, A. Hundt, M. Lowisch, M. Rabe, and F. Henneberger, Phys. Rev. Lett. **86**, 3172 (2001).

[20] M. Tadić, F. M. Peeters and K. L. Janssens, Phys. Rev. B **65**, 165333 (2002).

[21] Y. Chen, B. Gil, P. Lefebvre, H. Mathieu, T. Fukunaga, and H. Nakashima, *Excitons in Confined Systems*, Proceedings in Physics 25 (Springer, New York, 1988).

[22] A. Franceschetti, L. W. Wang, H. Fu, and A. Zunger, Phys. Rev. B **58**, R13367 (1998).

[23] S. V. Goupalov and E. L. Ivchenko, Phys. Solid State **43**, 1791 (2001).

[24] S. V. Goupalov, Phys. Rev. B **74**, 113305 (2006).

[25] B. Patton, W. Langbein, and U. Woggon, Phys. Rev. B **68**, 125316 (2003).

[26] M. Bayer, G. Ortner, O. Stern, A. Kuther, A. A. Gorbunov, A. Forchel, P. Hawrylak, S. Fafard, K. Hinzer, T. L. Reinecke, S. N. Walck, J. P. Reithmaier, F. Klopf, and F. Schäfer, Phys. Rev. B **65**, 195315 (2002).

[27] Y. Léger, L. Besombes, L. Maingault, D. Ferrand, and H. Mariette, Phys. Rev. B **72**, 241309(R) (2005).

[28] Y. Léger, L. Besombes, J. Fernández-Rossier, L. Maingault, and H. Mariette, Phys. Rev. Lett. **97**, 107401 (2006).

[29] D. N. Krizhanovskii, A. Ebbens, A. I. Tartakovskii, F. Pulizzi, T. Wright, M. S. Skolnick, and M. Hopkinson, Phys. Rev. B **72**, 161312(R) (2005).

[30] U. Rössler, S. Jorda, and D. Broido, Solid State Commun. **73**, 209 (1990).

[31] E. L. Ivchenko, *Optical Spectroscopy of Semiconductor Nanostructures* (Springer, New York, 2004).

[32] Y. Léger, L. Besombes, L. Maingault, D. Ferrand, and H. Mariette, Phys. Rev. Lett. **95**, 047403 (2005).

[33] F. Long, W. E. Hagston, P. Harrison, and T. Stirner, J. Appl. Phys. **82**, 3414 (1997).

[34] A. Messiah, *Mécanique Quantique* (Dunod, Paris, 1959).